

# Relating Scratch Resistance to Injection Molding-Induced Morphology of Polypropylene

Yutaka Kobayashi,<sup>1,2</sup> Yasuhiko Otsuki,<sup>1</sup> Hiroaki Kanno,<sup>3</sup> Yasuhiro Hanamoto,<sup>3</sup>  
Toshitaka Kanai<sup>2,4</sup>

<sup>1</sup>Research & Development Division, Prime Polymer Company, Limited, 580-30 Nagaura, Sodegaura-City, Chiba 299-0265, Japan

<sup>2</sup>Division of Material Sciences, Graduate School of Natural Science & Technology, Kanazawa University, Kakuma-Machi, Kanazawa-City, Ishikawa 920-1192, Japan

<sup>3</sup>Analysis Research Laboratories, Mitsui Chemical Analysis & Consulting Service Incorporated, 580-30 Nagaura, Sodegaura-City, Chiba 299-0265, Japan

<sup>4</sup>Research & Development Laboratory, Idemitsu Kosan Company, Limited, Anasaki-Kaigan, Ichihara-City, Chiba 299-0193, Japan

Received 26 June 2010; accepted 7 August 2010

DOI 10.1002/app.33142

Published online 11 October 2010 in Wiley Online Library (wileyonlinelibrary.com).

**ABSTRACT:** The relationship between the scratch resistance and the injection molding-induced morphology of polypropylene (PP) was investigated. The crystal structure near the surface was controlled by the mold temperature and the doping of a nucleating agent (NA). Although  $\alpha$ - and  $\beta$ -NA were used to improve the scratch resistance of PP that was molded at a mold temperature of 40°C, both of the NAs only slightly affected the scratch resistance due to low crystallinity at the surface. When the mold temperature was increased, the skin layer became thin and a  $\beta$ -form crystal formed. Plastic deformation under the scratch

was limited in the frozen layer. Consequently, the thickness of the frozen layer (which had low crystallinity) had the predominant effect on the scratch resistance in comparison to the polymorphism differences. The crystal morphology was analyzed with synchrotron micro-beam wide angle X-ray diffraction and Fourier transform infrared spectroscopy. © 2010 Wiley Periodicals, Inc. *J Appl Polym Sci* 120: 141–147, 2011

**Key words:** microdeformation; injection molding; morphology; poly(propylene)

## INTRODUCTION

Polypropylene (PP) is widely used in the automotive industry and is processed by injection molding, which induces a hierarchical morphology in molded parts. A large amount of research has been conducted with respect to the relationship between the injection molding-induced morphology and the resulting mechanical properties.<sup>1,2</sup> We have investigated properties at the surface of injection-molded plaques because controlling the surface properties is important to the industry.<sup>3–6</sup> The morphology near the surface is formed just behind the advancing flow front. The melt of PP is subjected to extensional deformation during the fountain flow, and is oriented parallel to the surface.<sup>3</sup> After contacting the cold wall of a tool, the melt is quenched. The crystallinity at a depth of 1  $\mu\text{m}$  is negligible, even if a nucleating agent (NA) is doped. Because the cooling rate is

slow at a distance far from the surface, the crystallinity increases in the depth direction.<sup>4</sup> Consequently, the microhardness of injection-molded specimens is lowest at the surface, although superstructure-like cross-hatching affects the hardness.<sup>5</sup> For a blend of PP and rubber, both the crystallinity and the rubber morphology reduce the shear strength at the surface.<sup>6</sup> The purpose of this study is to create a method to improve scratch resistance, which is considered to be the practical hardness at the surface in automotive parts.

The relationship between the scratch resistance and the injection molding-induced morphology has been investigated with respect to different polymer attributes and injection-molding conditions.<sup>7–10</sup> If the molecular weight (MW) and surface crystallinity of PP are high, the scratch performance improves when using the experimental method of a critical load.<sup>7</sup> From the damaged shapes on the scratched surface (e.g., the maximum depth of the scratch), low MW PP is characterized by superior resistance to scratch damage compared to high MW PP.<sup>8</sup> When using scratch test methods, the scratch resistance has an opposite dependency on the MW.<sup>9</sup> The most critical parameters that influence the scratch performance of

Correspondence to: Y. Kobayashi (Yutaka.Kobayashi@advcmp.com).

plastics are the yield stress and the coefficient of adhesive friction. Increasing the Young's modulus of the plastics does not necessarily improve the overall scratch performance.<sup>10</sup> Although previous studies have characterized the structures and physical properties of scratched specimens, the characteristics are averaged from the surface to the center in the depth direction. For this reason, the effects of injection molding-induced morphology on the scratch resistance are not clear near the surface.

In this study, we focus on the morphology of a frozen layer in the skin-core structure and its effect on the scratch resistance. The crystallinity of PP in the frozen layer was controlled by the mold temperature and a NA. The injection molding-induced morphology was analyzed using a polarizing optical microscope (POM), wide angle X-ray diffraction (WAXD), laser scanning microscopy (LSM), and Fourier transform infrared spectroscopy (FTIR). The scratch resistance was measured with a five-finger scratch tester.

## EXPERIMENTAL

### Materials and molding conditions

In this study, the PP was a Ziegler-Natta isotactic homopolymer (MFR 30 g/10min for 2.16 kg at 230°C, pentad fraction 97%) with a weight average molecular weight of 200 kg/mol and Mw/Mn ratio of 4.0. The  $\alpha$ -specific NA was sodium 2,2'-methylene-bis(4,6-di-*t*-butylphenylene)-phosphate (ADEKA Corp., NA-11).<sup>11</sup> The  $\beta$ -specific NA was N,N'-dicyclohexylnaphthalene-2,6-dicarboxamide (Shin Nihon Rika, NU 100).<sup>12</sup> The PP and 0.1 wt % of the NA were mixed with a twin-screw extruder (TEM-30, Toshiba Machine) with a barrel temperature of 200°C. Hereafter, the three types of PP are referred to as non-NAPP,  $\alpha$ -NAPP, and  $\beta$ -NAPP, respectively.

As shown in Figure 1, two types of plaques were used: Plaque 1 and Plaque 2. To study the crystallinity that was controlled by the NA doping, Plaque 1 (<sup>w</sup>70 mm × <sup>l</sup>270 mm × <sup>t</sup>3mm) was molded with an injection-molding machine (Toshiba, IS100F-III). The molding conditions were as follows: a mold temperature of 40°C, a barrel temperature of 200°C, a filling time of 3 s, a holding time of 8 s, and a cooling time of 20 s. The injection pressure was controlled automatically to maintain a constant injection velocity. The holding pressure was manually adjusted to 70% of the filling pressure. To study the crystallinity that was controlled by the mold temperature, Plaque 2 (<sup>w</sup>80 mm × <sup>l</sup>80 mm × <sup>t</sup>3mm) was molded with the following conditions: a barrel temperature of 200°C, a filling time of 1 s, a holding time of 20 s, and a cooling time of 360 s. The mold temperatures were

set to 20, 65, and 100°C with a high-pressure water circulation temperature controller.

### Morphological characterization

The molded specimens were characterized by using four types of experimental techniques; POM, WAXD, FTIR, and LSM. The POM observation was performed with an Olympus BH-2 at room temperature. A schematic of the setup is shown in Figure 1. The morphology of the microtomed section was observed parallel to the flow direction (edge view). The cross section of the scratched surface was observed perpendicular to the flow direction (end view).

The crystal morphology near the surface in the WAXD experiment was analyzed using synchrotron radiation at beam line, BL24XU of SPring-8 at Japan Synchrotron Radiation Research Institute (JASRI). The instrument used a light collection optical system with zone plates and a detector system with image plates (Rigaku R-AXIS). The square-shaped microbeam had dimensions of 0.273  $\mu\text{m}$  × 0.389  $\mu\text{m}$  and a wavelength of 1.2398 Å (10 keV). The PP specimens were mounted 52.3 mm from the image plate. The positions of Plaque 1 are shown in Figure 1. The measurements were performed at room temperature with the microbeam along the flow direction (edge view) and at distances of 1, 5, 20, 100, and 200  $\mu\text{m}$  from the surface along the normal direction in the specimens. The effects of the mold temperature in Plaque 2 could not be investigated with the microbeam X-ray method because the beam size was too small to measure heterogeneous morphology at the surface. A Rigaku RINT 2550 with an imaging plate was used to analyze the Plaque 2 that was molded at the specified mold temperatures. The circle-shaped beam had a radius of 0.15 mm and a wavelength of 1.54059 Å (CuK $\alpha$ , 40 kV, 370 mA). The measurements were performed at room temperature with the beam along the flow direction (edge view), and the X-ray beam was irradiated from the surface to a depth of 0.15 mm depth in the specimens.

All of the X-ray data were corrected for background (air and instrument) scattering before analysis. The crystallinity was calculated as the ratio between the integral of intensities diffracted by the crystalline part and the total integral of intensities,<sup>13</sup> i.e., a relative value related to the maximum crystallinity measured in the part. Although the PP exhibited polymorphism, crystallinity included all of the crystal forms:  $\alpha$ ,  $\beta$ , and  $\gamma$ . The  $\beta$ -ratio is defined as follows:  $(300)/((300) + (110) + (040) + (130))$ , where (110), (040), and (130) are the intensities of the lattice planes in the  $\alpha$ -form crystal on the 1D WAXD

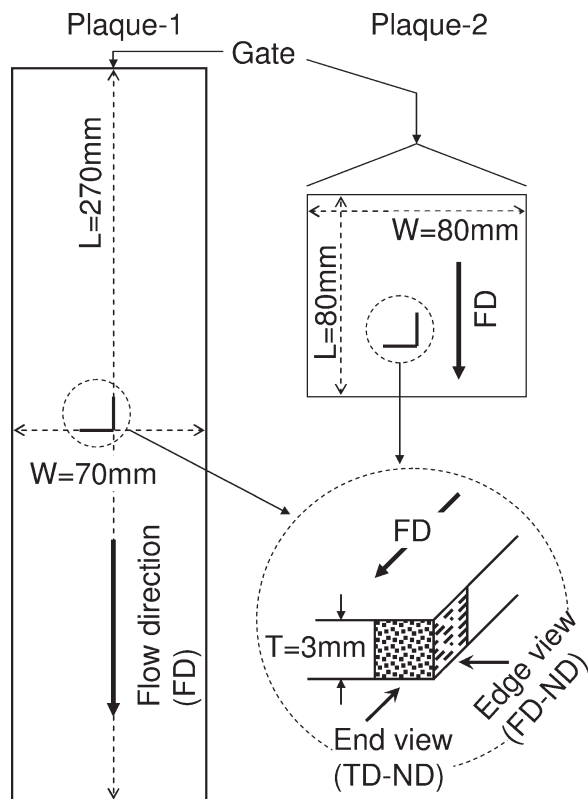


**Figure 1** A schematic diagram of the injection molded plaques and the observed specimens. Plaque 1: 270 mm  $\times$  70 mm  $\times$  3 mm, and Plaque 2: 80 mm  $\times$  80 mm  $\times$  3 mm.

profile, and (300) is the intensity of a characteristic lattice plane in the  $\beta$ -form crystal.

The FTIR experiment was performed with a Nicolet 8700 and Continuum Microscope at room temperature. The equipment was operated in transmission mode with 100 scans per sample at a resolution of  $1 \text{ cm}^{-1}$  in the wavenumber range between 4000 and  $650 \text{ cm}^{-1}$ . The positions of the specimen were the same as those for the POM experiment. The microtomed cross section of the specimen (40- $\mu\text{m}$  thickness) was measured with an aperture size of  $30 \mu\text{m} \times 150 \mu\text{m}$  in the normal direction. All of the spectra were collected for background spectra to remove atmospheric effects, such as carbon dioxide and the moisture in the air. The scratched surface was analyzed with an LSM, Lasertec OPTELICS H1200. Microphotographs were taken by using a green ray (546-nm wavelength). The measured positions were indicated for each case.

#### Measurement of the scratch resistance

The scratch resistance was evaluated with a five-finger scratch tester (Ford Lab Test Method BN108-13).<sup>14</sup> The tip of each scratch pin was a steel ball with a diameter of 1.0 mm. On the plaque, four pins were loaded with different weights to exert forces of

5, 10, 15, and 20 N, respectively. The scratching velocity was approximately 100 mm/s. The width and depth of the scratch were measured with the POM and LSM.

## RESULTS AND DISCUSSION

### Effect of nucleating agents on the scratch resistance

To increase stiffness of PP, an NA is typically doped. We have previously studied the surface morphology of PP with  $\alpha$ -NA and  $\beta$ -NA.<sup>4</sup> As shown in Figure 2, the crystal morphology in the injection-molded specimens was modified by adding NAs. Although large spherulites were observed in the non-NAPP, the  $\alpha$ -NAPP and  $\beta$ -NAPP did not exhibit large spherulites due to increasing nucleation. The crystallinity near the surface was measured with a microbeam synchrotron WAXD with beam dimensions of  $0.273 \mu\text{m} \times 0.389 \mu\text{m}$ . Table I shows the crystallinity at distances of 1, 5, 20, 100, and 200  $\mu\text{m}$  from the surface for the three samples. Because only

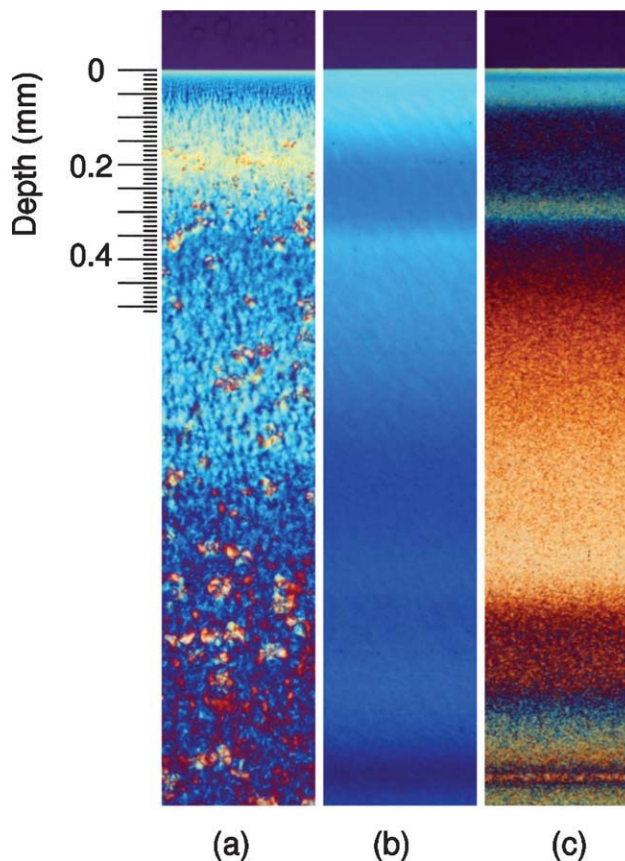


**Figure 2** Polarized optical microphotographs of injection-molded specimens: (a) non-NAPP, (b)  $\alpha$ -NAPP, and (c)  $\beta$ -NAPP. The micrographs were taken along the flow direction with the specimen rotated by  $45^\circ$  from the direction of the polarizer. [Color figure can be viewed in the online issue, which is available at [wileyonlinelibrary.com](http://wileyonlinelibrary.com)]



**TABLE I**  
Crystallinity of the Non-NAPP,  $\alpha$ -NAPP, and  $\beta$ -NAPP that Was Measured with WAXD

Depth ( $\mu\text{m}$ )	Crystallinity (%)		
	Non-NAPP	A-NAPP	$\beta$ -NAPP
1	Mesophase	Mesophase	Mesophase
5	Mesophase	A few $\alpha$ -form	A few $\alpha$ -form
20	A few $\alpha$ -form	37	34 (negligible)
100	46	61	62 (0.77)
200	62	68	65 (0.85)

( ):  $\beta$ -form ratio.

a mesomorphic-crystal was observed at a depth of 1  $\mu\text{m}$ , the NAs did not function under quenching conditions. The  $\beta$ -NA generated an  $\alpha$ -form crystal at a depth of 5–20  $\mu\text{m}$  and a  $\beta$ -form one from a depth of 100  $\mu\text{m}$  to the center of the specimen. The crystallin-

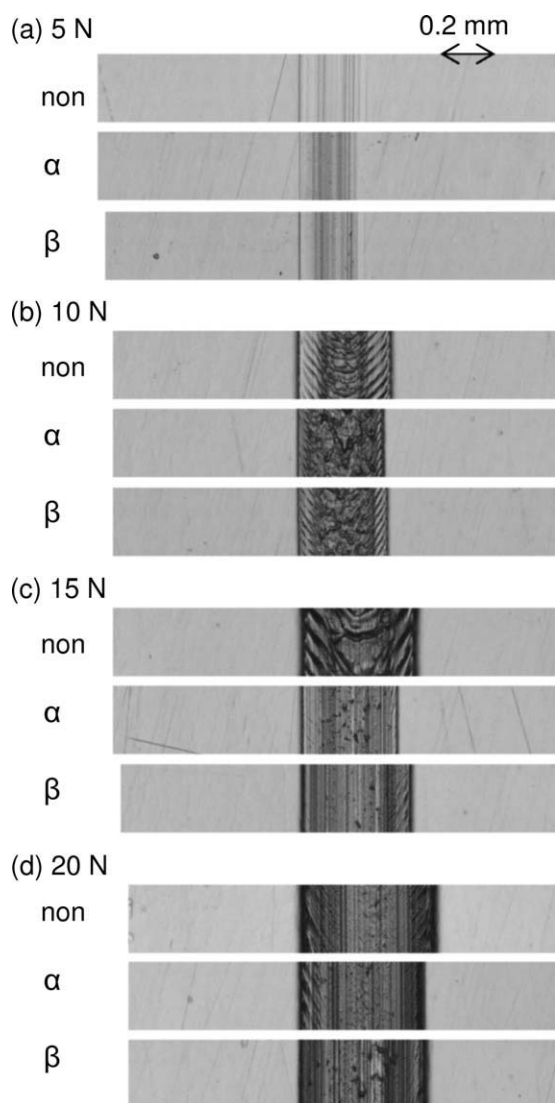


**Figure 3** LSM micrograph of non-NAPP,  $\alpha$ -NAPP, and  $\beta$ -NAPP after applying a load of (a) 5 N, (b) 10 N, (c) 15 N, and (d) 20 N.

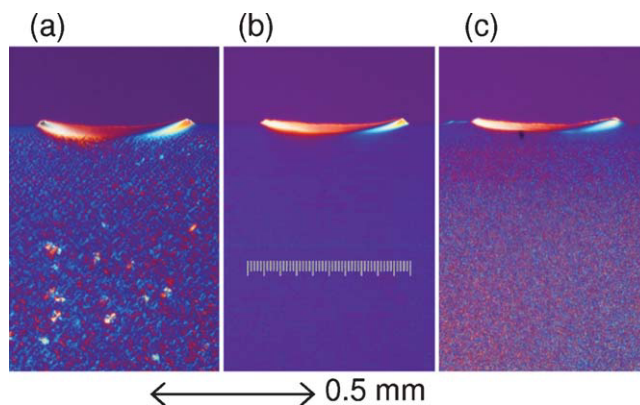


**Figure 4** Polarized optical microphotographs of (a) non-NAPP, (b)  $\alpha$ -NAPP, and (c)  $\beta$ -NAPP after the scratch test with an applied load of 15 N. [Color figure can be viewed in the online issue, which is available at [wileyonlinelibrary.com](http://wileyonlinelibrary.com)]

ity of the non-NAPP near the surface was lower than that of the NAPPs. The effects of the differences in scratch resistance were investigated.

Figure 3 shows the surface that was subjected to the five-finger scratch test with forces of 5, 10, 15, and 20 N. The scratches were observed with the LSM. At 5 N, traces were scarcely visible. A wedge-like pattern was formed at 10 and 15 N. The scratch behavior at 20 N was a ploughing type, i.e., scratched surface roughness was minor, and the scratched surface was smooth throughout the process. Because the scratch resistance of the three materials was equivalent, the NAs did not increase the hardness of the surface. Plastic deformation due to scratching was observed from the surface to a depth of 50  $\mu\text{m}$ , as shown in Figure 4. As mentioned earlier, the crystallinity near the surface was lower than that in the core area, and the NAs only slightly improved this. As a result, the scratch resistance of the injection-molded surface was not modified with the NAPPs. Controlling crystallinity near the surface is required; therefore, the mold temperature is investigated in the next section.

#### Mold temperature dependency of the surface morphology

Molten PP is extensionally stretched by the fountain flow mechanism and immediately freezes after contacting the cold wall in injection molding.<sup>4</sup> To increase the crystallinity at the surface, the effects of the mold temperature were investigated. Figure 5 shows the morphology of the non-NAPP near the surface in the plaques that were molded at three temperatures. At a mold temperature of 20°C, the thickness of the skin layer was 0.2 mm and  $\beta$ -form spherulites were observed in the core region. When the mold temperature was increased, the skin

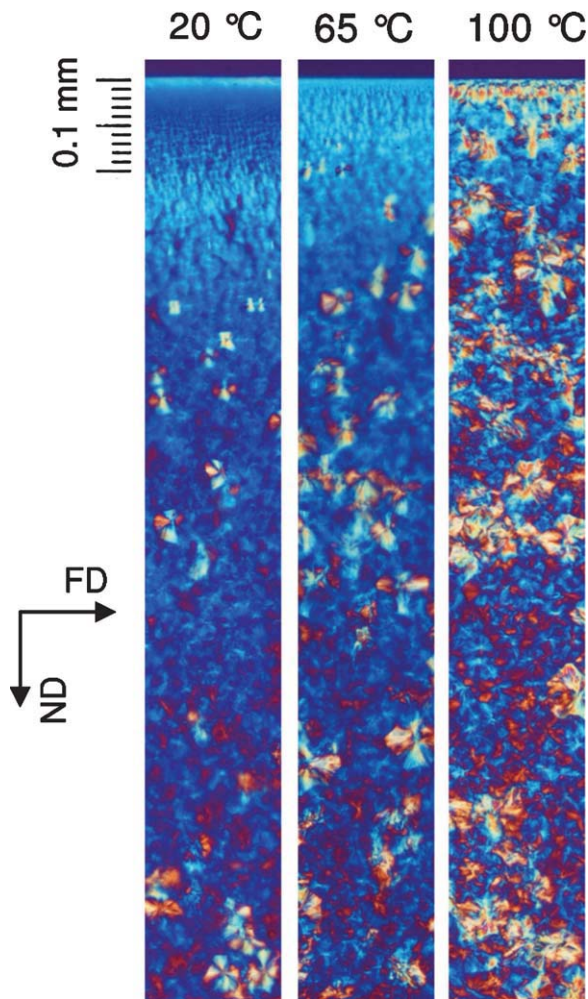


**Figure 5** Changes in the crystal structure with the mold temperature. The morphology of the cross section in the edge view using a POM. The micrograph was taken along the flow direction with the specimen rotated by 45° from the direction of the polarizer. [Color figure can be viewed in the online issue, which is available at [wileyonlinelibrary.com](http://www.interscience.wiley.com)]

thickness decreased and transcrystalline  $\beta$ -form appeared near the surface at 100°C. The  $\beta$ -form crystal was quantified from the 1D WAXD patterns, see Figure 6. The  $\alpha$ -form crystal is identified by the (110), (040), (130), (111), and (131)+(041) lattice planes, while the  $\beta$ -form crystal is identified by the (300) lattice plane.<sup>15</sup> The  $\beta$ -form ratio at the 100°C mold temperature was 0.4 in the region from the surface to a depth of 0.15 mm. At the mold temperatures of 20 and 65°C, the  $\beta$ -form crystal was not detected near the surface by the WAXD.

The crystal structure in the depth direction was analyzed with FTIR. Figure 7 shows changes in the relative absorbance of A998/A973 and A841/A973, which were measured from the surface to the center at 0.2 mm intervals. The relative absorbance is commonly used to determine the crystallinity of PP.<sup>16</sup> IR bands of 973, 998, 841, and 1220  $\text{cm}^{-1}$  correspond

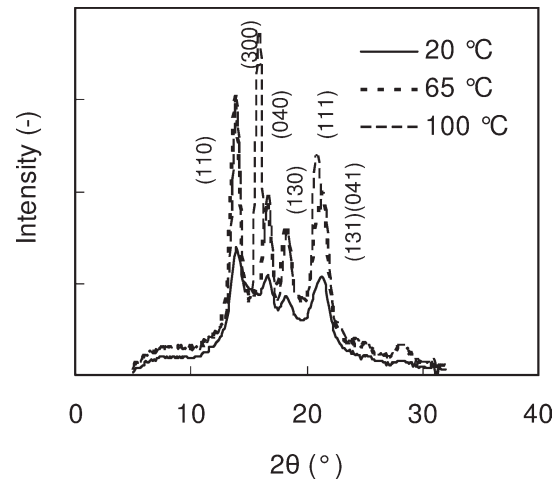


**Figure 6** Changes in the 1D WAXD patterns due to the mold temperature at a depth of 0.15 mm in the cross section. The WAXD patterns were taken with an edge view, a beam diameter of 0.3 mm and at room temperature.

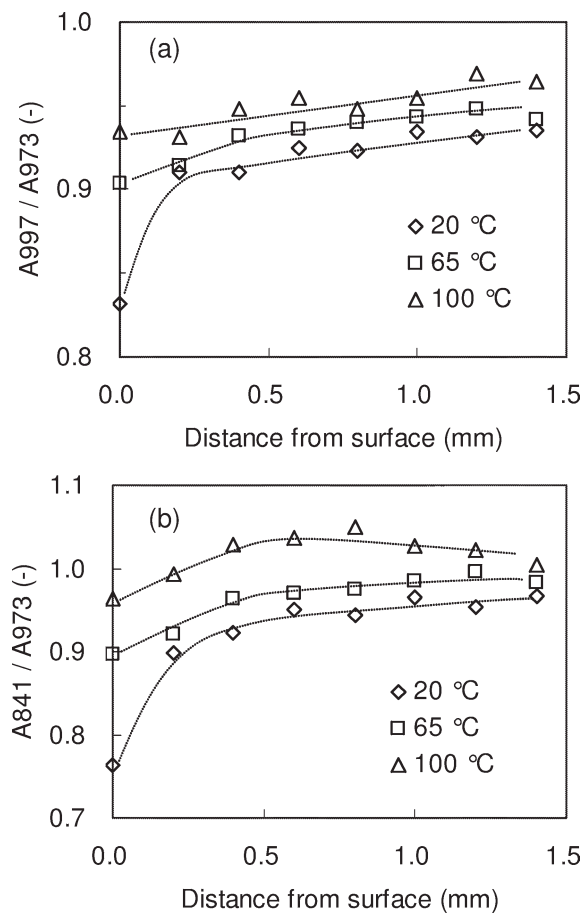


**Figure 7** Changes in the relative absorbance of the IR spectra related to monomer units in the helical sequences of PP: (a) A997/A973 and (b) A841/A973. The measurements were taken from the surface to the center of the sample at 0.2 mm intervals. The spectra were taken with an edge view, an aperture size of 30  $\mu\text{m} \times 150 \mu\text{m}$  and at room temperature.

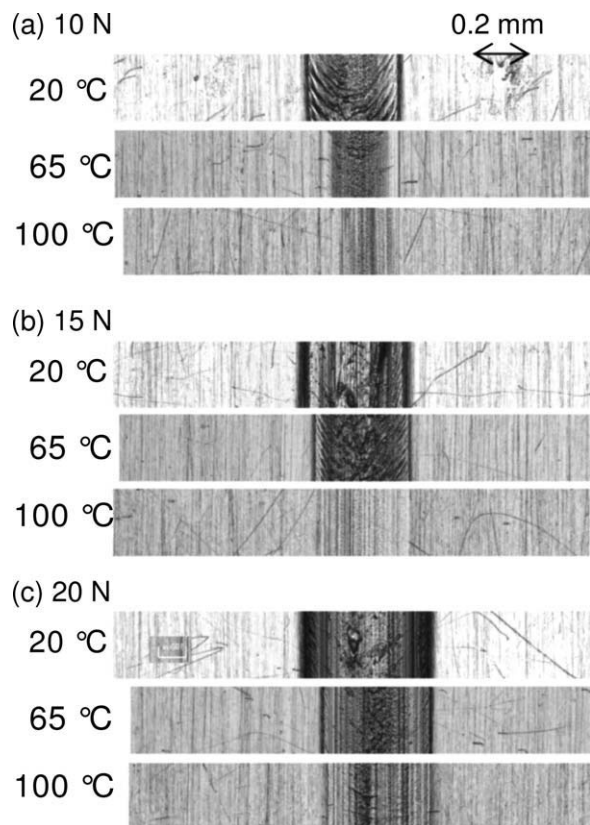


**Figure 8** LSM micrograph of PP that was molded at mold temperatures of 20, 65, and 100°C after applying a load of (a) 10 N, (b) 15 N, and (c) 20 N.

to helical structures and the minimum  $n$  values of those bands are 5, 10, 12, and 14 monomer units in helical sequences, respectively.<sup>17,18</sup> The depth profile of A998/A973 at 20°C changed in a depth of 0.2 mm, which was in agreement with the morphological changes that were observed by the POM. The absorbance of A841/A973 increased gradually from the surface to a depth of 0.4 mm. A possible cause is that it is difficult to form long helical sequences (minimum  $n = 12$ ) under a rapid cooling condition. In the next section, crystallinity, polymorphism and their depth profiles are compared to the scratching phenomena.

#### Effect of mold temperature on the scratch resistance

As shown in Figure 8, the traces formed by the five-finger scratch tester on the injection-molded plaques were observed with the LSM. When a force of 15 N was applied to the plaques, the grooves appeared differently: mar at 100°C, wedge formation at 65°C, and plowing at 20°C. The scratch width is a suitable parameter that can be used to quantify the appearance.<sup>9</sup> As shown in Figure 9(a), the width decreased as the mold temperature increased. Because a high hardness was observed at a high mold temperature,

crystallinity near the surface was measured by using WAXD and FTIR. Figure 9(b) shows the relationship between the width and the crystallinity from the surface to a depth of 0.15 mm that was measured with WAXD. Although the crystallinity at mold temperatures of 45 and 100°C was approximately 60%, the corresponding widths were different at 10N. The relative intensity (A841/A973) was measured from the surface to a depth of 50  $\mu\text{m}$  with FTIR, which is another factor of the crystallinity. By comparing Figure 9(b,c), the relative intensity is roughly proportional to the width: thus, the depth at which the

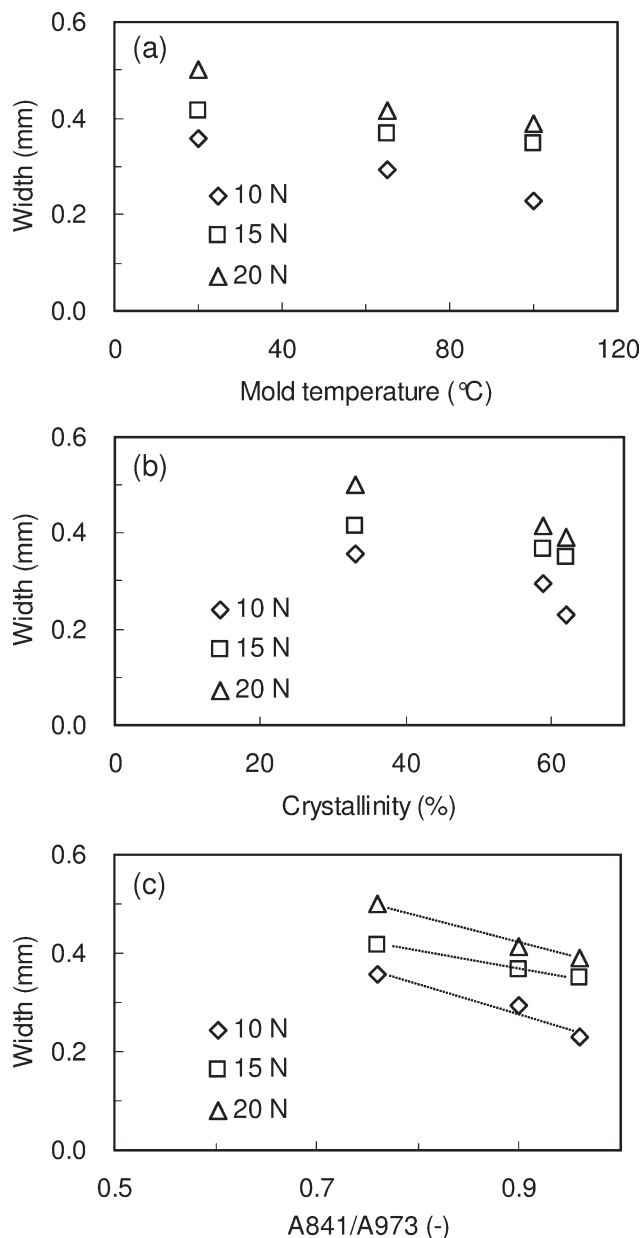


**Figure 9** Changes in the scratch width of PP that was molded at mold temperatures of 20, 65, and 100°C after applying a load of 10, 15, and 20 N. Horizontal axis: (a) mold temperature, (b) crystallinity, and (c) relative absorbance of A841/A973.



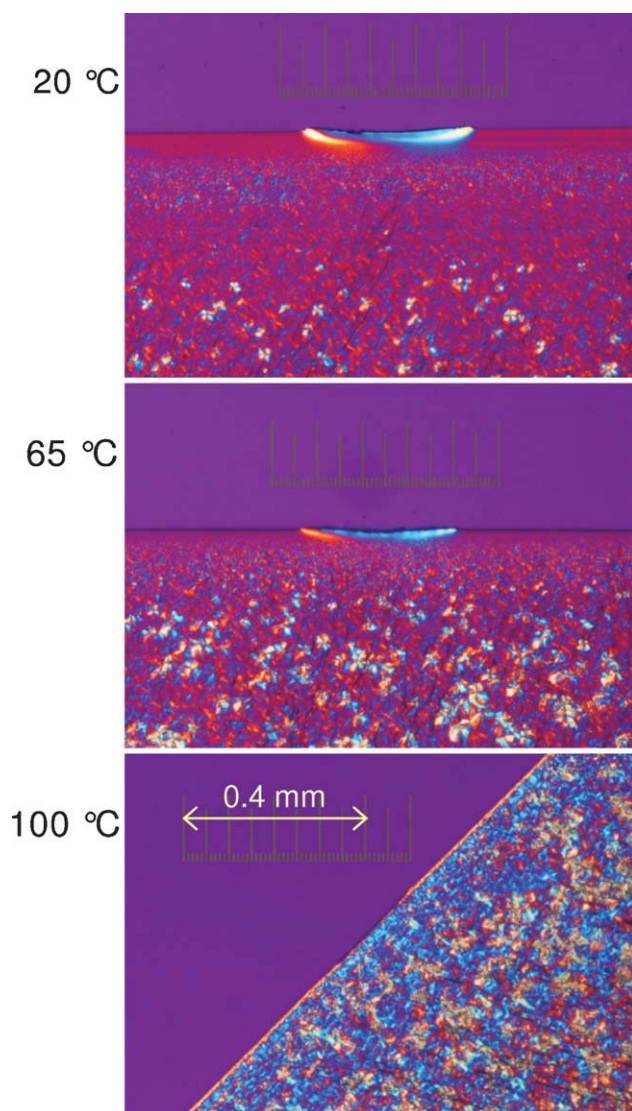


**Figure 10** Polarized optical microphotographs of PP that was molded at mold temperatures 20, 65, and 100°C after the scratch test with an applied load of 15 N. [Color figure can be viewed in the online issue, which is available at [wileyonlinelibrary.com](http://www.interscience.wiley.com)]

crystallinity is measured is important. At 20 and 65°C, the molten polymer in contact with the mold surface froze immediately: few spherulites appeared in this frozen layer. At 100°C, the frozen layer was not observed as it was in Figure 5. Although the formation of a  $\beta$ -form crystal was mentioned earlier, the thickness of the frozen layers was found to be predominant over the scratch resistance in this study. Figure 10 shows a cross section of the scratched plaques. Plastic deformation was observed inside of the groove, and the deformed area coincided with the thickness of the frozen layer. Although the skin of the specimen at 100°C was scraped, plastic deformation was not observed near the surface. As a result, increasing the crystallinity at

the surface is an effective means to improve the scratch resistance. However, the common method of adding an NA to PP does not result in increased scratch performance for injection molding.

## CONCLUSIONS

The relationship between the crystal morphology near the surface of injection-molded PP and the scratch resistance was investigated in this study. Doping a NA into PP did not improve the scratch resistance because the crystallinity near the surface of NAPP was very low. To increase the crystallinity, a high mold temperature was effective. However, a  $\beta$ -form crystal was simultaneously formed at the surface. In conclusion, the thickness of the frozen layer which has lower crystallinity was predominant in the scratch resistance in comparison to the polymorphism differences.

We thank K. Tanaka for assistance with the FTIR analysis and T. Tanaka for the injection molding. Prime Polymer is acknowledged for allowing the release of this study.

## References

1. Fujiyama, M. In: Polypropylene; Karger-Kocsis, J., Ed.; Chapman & Hall: London, 1995; Vol. 1, p 167.
2. Phillips, R. A.; Wolkowicz, M. D.; In: Polypropylene Hand Book, 2nd ed.; Pasquini, N., Ed.; Carl Hanser Verlag: Munich, 2005; Chapter 3, pp 147–264.
3. Kobayashi, Y.; Otsuki, Y.; Kanai, T. *Polym Eng Sci*, to appear.
4. Kobayashi, Y.; Otsuki, Y.; Kanno, H.; Sasakawa, T.; Hanamoto, Y.; Kanai, T. *Polym Eng Sci*, to appear.
5. Kobayashi, Y.; Kanno, H.; Hanamoto, Y.; Ando, M.; Kanai, T. *J Appl Polym Sci* 2010, 116, 1823.
6. Kobayashi, Y.; Ando, M.; Kanai, T. *J Appl Polym Sci* 2010, 116, 2590.
7. Moghbelli, E.; Browning, R. L.; Boo, W.-J.; Hahn, S. F.; Feick, L. J. E.; Sue, H.-J. *Tribol Int* 2008, 41, 425.
8. Hadal, R. S.; Misra, R. D. K. *Mater Sci Eng A* 2005, 398, 252.
9. Wong, M.; Lim, G. T.; Moyses, A.; Reddy, J. N.; Sue, H.-J. *Wear* 2004, 256, 1214.
10. Jiang, H.; Lim, G. T.; Reddy, J. N.; Whitcomb, J. D.; Sue, H.-J. *J Polym Sci B* 2007, 45, 1435.
11. Urushihara, T.; Okada, K.; Watanabe, K.; Tada, A.; Tobita, E.; Kawamoto, N.; Hikosaka, M. *Polymer J* 2007, 39, 55.
12. Chvátlová, L.; Navrátilová, J.; Čermák, R.; Raab, M.; Obadal, M. *Macromolecules* 2009, 42, 7413.
13. Natta, G.; Corradini, P.; Cesari, M. *Atti della Accademia nazionale dei Lincei, Rendiconti* 1957, 22, 11.
14. Chu, J.; Ruma, L.; Coleman, B. *Polym Eng Sci* 1996, 38, 38.
15. Housmans, J. W.; Gahleitner, M.; Peters, G. W. M.; Meijer, H. E. H. *Polymer* 2009, 50, 2304.
16. Law, A.; Simon, L.; Lee-Sullivan, P. *Polym Eng Sci* 2008, 48, 627.
17. Zhu, X. Y.; Yan, D. Y.; Fang, Y. P. *J Phys Chem B* 2001, 105, 12461.
18. An, H.; Zhao, B.; Ma, X.; Shao, C.; Wang, X.; Fang, Y.; Li, L.; Li, Z. *Macromolecules* 2007, 40, 4740.